Inelastic J/ψ production in polarized photon-hadron collisions

Feng Yuan, Hui-Shi Dong and Li-Kun Hao
Department of Physics, Peking University, Beijing 100871, People's Republic of China

Kuang-Ta Chao
China Center of Advanced Science and Technology (World Laboratory), Beijing 100080, People's Republic of China
and Department of Physics, Peking University, Beijing 100871, People's Republic of China

Abstract

Presented here is a calculation of inelastic J/ψ production in polarized photon-hadron collisions under the framework of NRQCD factorization formalism. We consider the photoproduction of J/ψ in the energy range relevant to HERA. The Weizsäcker-Williams approximation is adopted in the evaluation of the cross sections for ep collisions. We found that this process can give another independent test for the color-octet mechanism, and the different features for the two color-octet processes may provide further informations on the mechanism for inelastic J/ψ photoproduction. And the discrepancy on the production asymmetry A between various sets of polarized gluon distribution functions is also found to be distinctive.

PACS number(s): 12.40.Nn, 13.85.Ni, 14.40.Gx

I. INTRODUCTION

The nucleon spin structure has attracted a lot of attention in the last ten years since the discovery of the so-called "spin crisis" by the European Muon Collaboration (EMC) [1]. During these times, much has been done to understand the spin structure of proton both on the theoretical side and the experimental side (mostly from the polarized DIS data). However, the use of DIS data alone does not allow an accurate determination for the polarized parton densities, especially for the polarized gluon distribution, which is crucial important to understand the gluon contribution to the proton spin. And now, the upgrade of HERA collider with polarized electron beam and proton beam at $\sqrt{s} = 300GeV$ in the near future has been considered for a long time [2]. With this high energy polarized electron-proton collider, one can investigate the polarized structure functions in much broader range of x and Q^2, especially, to very low x and high Q^2 region. And also the exploration of polarized gluon distribution $\Delta G(x, Q^2)$ will become accessible. To determine $\Delta G(x, Q^2)$, various photon-gluon fusion processes can be used. The typical promising process for this purpose is the large$-p_T$ di-jet production [2], which is a gluon induced process even in the leading order (LO) of QCD calculations. However, for this process one must deal with the uncertainty arising from the resolved photon contributions. In this paper, we will consider the inelastic J/ψ production in the polarized photon-hadron collisions. Because the inelastic J/ψ photoproduction is also a gluon induced process, so this process can be viewed as a possible way to study the polarized gluon distribution in the proton. Furthermore, the resolved photon contribution to this process is negligible in the major kinematical region of the produced J/ψ. So, by inducing some kinematical cut, the uncertainties due to the resolved photon contribution can be eliminated safely.

On the other hand, studies of heavy quarkonium production in high energy energies is another hot topic in recent years. In the conventional picture, the heavy quarkonium production is described in the color-singlet model [3]. In this model, it is assumed that the heavy quark pair must be produced in a color-singlet state in short distance with the same angular-momentum quantum number as the charmonium meson which is eventually observed. However, with the recent Tevatron data on high p_T J/ψ production appearing, this color-singlet picture for heavy quarkonium production became questionable, The data is larger than the theoretical prediction of the color-singlet model by a factor of about $30 \sim 50$ [4]. This is called the J/ψ (ψ') surplus problem. On the theoretical side, the naive color-singlet model has been supplanted by the nonrelativistic QCD (NRQCD) factorization formalism [5], which allows the infrared safe calculation of inclusive charmonium production and decay rates. In this approach, the production process is factorized into short and long distance parts, while the latter is associated with the nonperturbative matrix elements of four-fermion operators. So, for heavy quarkonium production, the quark-antiquark pair does not need to be in the color-singlet state in the short distance production stage, which is at the scale of $1/m_Q$ (m_Q is the heavy quark mass). At this stage, it allows the other color configuration than the singlet for the heavy quark pair, such as color-octet. The later situation for heavy quarkonium production is called the color-octet mechanism. In this production mechanism, heavy quark-antiquark pair is produced at short distances in a color-octet state, and then hadronizes into a final state quarkonium (physical state) nonperturbatively. Provided this color-octet mechanism, one might provide explain the Tevatron

data on the surplus of J/ψ and ψ' production [6,7].

Even though the color-octet mechanism has achieved some successes in describing the production and decay of heavy quarkonia, more tests of this mechanism are still needed. Recently, the photoproduction data from HERA [8,9] puts a question about the universality of the color-octet matrix elements [10,11], in which the fitted values of the matrix elements $\langle \mathcal{O}_8^{J/\psi}(^1S_0)\rangle$ and $\langle \mathcal{O}_8^{J/\psi}(^3P_J)\rangle$ are one order of magnitude smaller than those determined from the Tevatron data [7]. (More recently, possible solutions for this problem have been suggested in [12,13].) In this situation it is certainly helpful to find other processes to test the color-octet mechanism in the heavy quarkonium production. So, the inelastic J/ψ production in polarized photon-hadron collisions can give another independent test of the production mechanism, aside from the unpolarized J/ψ.

The rest of the paper is organized as follows. In Sec. II, we will give the polarized cross section formula for the inelastic J/ψ production at the polarized electron-proton collider. Here, we adopt the Weizsäcker-Williams approximation to calculate the electroproduction cross section with the photoproduction cross section. The numerical results are given in Sec. III. We will display the polarized cross sections for both the polarized photon-proton collisions and the electron-proton collisions. All of our results are relevant to the energy range of the upgrade polarized HERA collider. We also study the J/ψ production asymmetry and its dependence on the polarized gluon distributions. In Sec. IV, we give the conclusions.

II. POLARIZED CROSS SECTION FORMULAS

In photoproduction processes, the electron-proton cross section can be equivalent to the photoproduction cross section convoluted by the photon flux factor from the electron under the Weizsäcker-Williams approximation [14],

$$d\sigma_{ep} = \int dy f_\gamma^{(e)}(y) d\sigma_{\gamma p}. \tag{1}$$

Here, y is the energy fraction of the electron carried by the photon. $f_\gamma^{(e)}$ is the flux factor of photon (or the distribution function of photon in the electron). In the following calculations, we use the form from [15],

$$f_\gamma^{(e)}(y) = \frac{\alpha_{em}}{2\pi}[\frac{1+(1-y)^2}{y}\log\frac{Q^2_{max}(1-y)}{m_e^2 y^2} + 2m_e^2 y(\frac{1}{Q^2_{max}} - \frac{1-y}{m_e^2 y^2})], \tag{2}$$

where m_e is the electron mass, and Q^2_{max} is the maximum value of Q^2 for the photoproduction processes. In the following numerical calculations, we will adopt $Q^2_{max} = 1GeV^2$. Compared with the original Weizsäcker-Williams function, the above equation contains a non-logarithmic term with a singular behavior at $y \to 0$ [15]. This term will give non-negligible contributions to the unpolarized cross section.

Correspondingly, the polarized electroproduction cross section has the similar form,

$$d\Delta\sigma_{ep} = \int dy \Delta f_\gamma^{(e)}(y) d\Delta\sigma_{\gamma p}, \tag{3}$$

where the polarized photon flux factor function $\Delta f_\gamma^{(e)}(y)$ has been derived in Ref. [16],

$$\Delta f_{\gamma}^{(e)}(y) = \frac{\alpha_{em}}{2\pi}[\frac{1-(1-y)^2}{y}\log\frac{Q^2_{max}(1-y)}{m_e^2 y^2} + 2m_e^2 y^2(\frac{1}{Q^2_{max}} - \frac{1-y}{m_e^2 y^2})]. \tag{4}$$

This function also contains a non-logarithmic term, which however is not singular at $y \to 0$. The numerical calculations show that this term will contribute about 5% to the total cross section of the inelastic J/ψ photoproduction at $\sqrt{s} = 300GeV$ for $Q^2_{max} = 1GeV^2$. The polarized cross section $\Delta\sigma$ in the above equation is defined in terms of $\sigma(\lambda_1, \lambda_2)$ with definite helicities for incoming particles,

$$d\Delta\sigma = \frac{1}{4}[d\sigma(+,+) + d\sigma(-,-) - d\sigma(+,-) - d\sigma(-,+)]. \tag{5}$$

In our study, we also adopt the Weizsäcker-Williams approximation described above to evaluate the inelastic photoproduction of J/ψ in electron-proton collisions. That is, the polarized and unpolarized cross sections for J/ψ production in electron-proton collisions have the following forms,

$$d\Delta\sigma(ep \to e + J/\psi + X) = \int_{y_{min}}^{y_{max}} dy \Delta f_{\gamma}^{(e)}(y) d\Delta\sigma(\gamma p \to J/\psi + X), \tag{6}$$

$$d\sigma(ep \to e + J/\psi + X) = \int_{y_{min}}^{y_{max}} dy f_{\gamma}^{(e)}(y) d\sigma(\gamma p \to J/\psi + X), \tag{7}$$

where y_{min} and y_{max} are the kinematical boundary for the photon energy fraction from the electron beam. In the above equation, we do not include the resolved photon contribution to the J/ψ photoproduction at ep colliders. This is because the resolved contribution is important only in the lower z region ($z < 0.2$) [17], where z is the energy fraction of the produced J/ψ. So, by inducing a lower bound cut on z, the resolved photon contribution can be eliminated. $\Delta\sigma(\gamma p \to J/\psi + X)$ is the polarized cross section for the inelastic production of J/ψ in the polarized photon-proton fusion processes.

At high energies, the photoproduction processes proceed predominantly through photon-gluon fusion. So, the polarized cross section $\Delta\sigma(\gamma p \to J/\psi + X)$ is related to the polarized gluon distributions in the proton,

$$d\Delta\sigma(\gamma p \to J/\psi + X) = \int dx \Delta G(x, Q^2) d\Delta\sigma(\gamma g \to J/\psi + X). \tag{8}$$

The polarized gluon distribution function $\Delta G(x, Q^2)$ is defined as usual way, and now there are various parametrizations for this quantity, such the GRVS sets [18], the GS sets [19], the DSS sets [20].

In photon-gluon fusion processes, according to the NRQCD factorization formalism, the unpolarized cross section and the polarized cross section can be factorized as the following forms,

$$d\sigma(\gamma + g \to J/\psi + X) = \sum_n F(\gamma + g \to n + X)\langle \mathcal{O}_n^{J/\psi}\rangle, \tag{9}$$

$$d\Delta\sigma(\gamma + g \to J/\psi + X) = \sum_n \Delta F(\gamma + g \to n + X)\langle \mathcal{O}_n^{J/\psi}\rangle. \tag{10}$$

Here, n denotes the $c\bar{c}$ pair configuration in the intermediate state (including angular momentum $^{2S+1}L_J$ and color index 1 or 8). $F(\gamma + g \to n + X)$ and $\Delta F(\gamma + g \to n + X)$ are

the short distance coefficients for the unpolarized and polarized cases respectively for the subprocess $\gamma + g \to n + X$. $\langle \mathcal{O}_n^{J/\psi} \rangle$ is the long distance non-perturbative matrix element which represents the probability of the $c\bar{c}$ pair in n configuration evolving into the physical state J/ψ. The short distance coefficients F and ΔF can be calculated by using perturbative QCD in expansion of powers of α_s. The long distance matrix elements are still not available from the first principles at present. However, the relative importance of the contributions from different terms can be estimated by using the NRQCD velocity scaling rules.

In order to suppress the diffractive contribution and higher-twist corrections, we induced the lower bound cut for the J/ψ transverse momentum $p_T > 1GeV$. With this constraints (non-zero p_T for J/ψ), there are the following $2 \to 2$ partonic processes contributing to J/ψ inelastic photoproduction in the photon-gluon fusion processes,

$$\gamma + g \to c\bar{c}(^3S_1, \underline{1}) + g, \tag{11}$$
$$\gamma + g \to c\bar{c}(^1S_0, \underline{8}) + g, \tag{12}$$
$$\gamma + g \to c\bar{c}(^3S_1, \underline{8}) + g, \tag{13}$$
$$\gamma + g \to c\bar{c}(^3P_J, \underline{8}) + g. \tag{14}$$

The first subprocess is the color-singlet process, and the last three processes are all the color-octet processes. The unpolarized cross sections for these processes have been calculated in literature [3,10,17]. The polarized cross section for the color-singlet process has also been calculated in [21].

To calculate the polarized cross sections for the color-octet processes, we employ the *helicity amplitude* method. With this method, one can calculate the cross sections $\sigma(\lambda_1, \lambda_2)$ with definite helicities for the incident particles. Following [22], we choose the polarization vectors for the incident photon, the incident gluon and the outgoing gluon as the following forms,

$$\not{\epsilon}_1^{(\pm)} = N_e[\not{p}_1 \not{p}_2 \not{p}_3(1 \mp \gamma_5) + \not{p}_3 \not{p}_2 \not{p}_1(1 \pm \gamma_5)], \tag{15}$$
$$\not{\epsilon}_2^{(\pm)} = N_e[\not{p}_2 \not{p}_3 \not{p}_1(1 \mp \gamma_5) + \not{p}_1 \not{p}_3 \not{p}_2(1 \pm \gamma_5)], \tag{16}$$
$$\not{\epsilon}_3^{(\pm)} = N_e[\not{p}_3 \not{p}_1 \not{p}_2(1 \mp \gamma_5) + \not{p}_2 \not{p}_1 \not{p}_3(1 \pm \gamma_5)]. \tag{17}$$

Where $p_1,\ p_2,\ p_3$ and $e_1,\ e_2,\ e_3$ are the momenta and the polarization vectors for the incident photon, incident gluon and outgoing gluon respectively. And the normalization factor N_e is

$$N_e = \frac{1}{\sqrt{2\hat{s}\hat{t}\hat{u}}}, \tag{18}$$

where the Mandelstam invariants $\hat{s},\ \hat{t},\ \hat{u}$ are defined as

$$\hat{s} = (p_1 + p_2)^2, \quad \hat{t} = (p_2 - p_3)^2, \quad \hat{u} = (p_1 - p_3)^2, \tag{19}$$

and they satisfy the relation

$$\hat{s} + \hat{t} + \hat{u} = M^2 = 4m_c^2.$$

With these definitions for the polarization vectors of the photon and gluons Eqs. (15)-(17), the calculations of the helicity amplitudes are straightforward. From these helicity amplitudes, we can easily get the cross sections with the definite helicities for the incident

particles. And then we can obtain the polarized cross sections $d\Delta\sigma(\gamma g \to J/\psi + X)$ for the different partonic processes Eqs. (12)-(14) from the definition Eq. (5). Their analytic expressions are listed in the Appendix. The unpolarized cross section for every partonic processes can also be obtained by summing up the cross sections with all of the possible helicity states for the external particles. We have checked that our results for the unpolarized cross sections are consistent with the results of Ref. [10,17]. For comparison, we also list the unpolarized cross sections in the Appendix.

After getting the polarized cross section, we can also calculate the asymmetry

$$A(\beta) = \frac{d\Delta\sigma/d\beta}{d\sigma/d\beta}, \tag{20}$$

where β represents for some kinematical parameters, such as J/ψ transverse momentum p_T and the energy fraction z. z is defined as $z = p \cdot k_{J/\psi}/p \cdot p_1$ with p, $k_{J/\psi}$, p_1 being the momenta of the proton, the outgoing J/ψ and the incident photon respectively. The production asymmetry parameter A is more efficiency than the polarized cross section $\Delta\sigma$ for the study of the polarized processes in the polarized collisions. This is because A is normalized, and then less depends on the input parameters which will strongly affect the normalization of the cross sections, such as the charm quark mass, strong coupling, and the factorization and renormalization scales.

III. NUMERICAL RESULTS

Provided the polarized and the unpolarized cross sections for the subprocesses, the inelastic J/ψ production rate and asymmetry in polarized photon-hadron collisions can be obtained. For the numerical evaluation, we choose the strong coupling constant α_s, the charm quark mass m_c, and the factorization scale μ^2 to be

$$\alpha_s = 0.3, \quad m_c = 1.5\ GeV, \quad \mu^2 = (2m_c)^2.$$

For the parton distribution function of the proton, we use the GRV LO parametrization [23]. For the polarized gluon distribution function, we will consider the GRVS sets [18], the GS sets [19], and the DDS sets [20].

We first display the different partonic processes contributions to the polarized cross section of J/ψ inelastic production, where we adopt the GRVS STD set as the default set for the polarized gluon distribution function of the proton. Fig. 1 is for the photon-proton collisions, where we typically set the energy of photon-proton system to be $W_{\gamma p} = 100GeV$ relevant to the photoproduction processes at HERA. Fig. 2 is for the electron-proton collisions, where we set the energy range also relevant to HERA, $\sqrt{s} = 300GeV$. For the electroproduction cross sections, the integral region of $W_{\gamma p}$ is set to be: $(25GeV)^2 < W^2_{\gamma p} < (180GeV)^2$ typically used in the photoproduction processes at HERA. In these two figures, we both plot the z and p_T^2 distributions: (a) are z distributions and (b) are p_T^2 distributions. To evaluate these curves, we have imposed a cut on z and P_T^2: $0.1 < z$ for the p_T^2 distributions and $P_T^2 > 1GeV^2$ for the z distributions. For the NRQCD long distance matrix elements, we set as

$$\langle \mathcal{O}_1^{\psi}(^3S_1)\rangle = 1.16 GeV^3, \tag{21}$$
$$\langle \mathcal{O}_8^{\psi}(^3S_1)\rangle = 1.06\times 10^{-2} GeV^3, \tag{22}$$
$$\langle \mathcal{O}_8^{\psi}(^1S_0)\rangle = 3.0\times 10^{-2} GeV^3, \tag{23}$$
$$\langle \mathcal{O}_8^{\psi}(^3P_0)\rangle/m_c^2 = 1.0\times 10^{-2} GeV^3, \tag{24}$$
$$\langle \mathcal{O}_8^{\psi}(^3P_J)\rangle = (2J+1)\langle \mathcal{O}_8^{\psi}(^3P_0)\rangle. \tag{25}$$

The last equation comes from the heavy quark spin symmetry of NRQCD. The color-singlet matrix element $\langle \mathcal{O}_1^{\psi}(^3S_1)\rangle$ can be related to the wave function at origin, and can be taken its value from the leptonic decay width of J/ψ. The value of the color-octet matrix element $\langle \mathcal{O}_8^{\psi}(^3S_1)\rangle$ is taken from a fit to the large p_T J/ψ production at the Tevatron [24]. This matrix element is not important to J/ψ photoproduction both for the unpolarized and polarized cases. On the other hand, the two other color-octet matrix elements, $\langle \mathcal{O}_8^{\psi}(^1S_0)\rangle$ and $\langle \mathcal{O}_8^{\psi}(^3P_0)\rangle$, are known to be very important in the inelastic J/ψ photoproduction [10,17]. However, their values are not well determined from the present experimental data on J/ψ productions. Here, we just follow Ref. [17] and take their values tentatively as listed above (which are also consistent with the naive NRQCD velocity scaling rules) to see what their contributions to the polarized cross section of the inelastic J/ψ photoproduction will be. The solid curves in these two figures are for the color-singlet process contributions, the dashed lines for the color-octet $^1S_0$ contributions, the dotted lines for the color-octet ^3P_J contributions, and the dotted-dashed lines for the color-octet $^3S_1$ contributions.

From Figs. 1 and 2, we can see that in the lower z region of the inelastic J/ψ production the dominant contribution comes from the color-singlet process. In the larger z region, the dominant comes from the color-octet $^1S_0$ process, and its contribution rise rapidly with z in the whole region. This property is as the same as that for the unpolarized cross section [10]. However, for the unpolarized cross section of inelastic J/ψ photoproduction, we know that this rapidly rising property at large z is not consistent with the experimental measurements [8]. It is argued in [17] that in this region, the soft gluon resummation is important, which may smear the z distribution in the large z region. So, the predictions for the LO calculations may be not reliable. Correspondingly, the predictions of the polarized cross section for the color-octet $^1S_0$ contributions (the dashed lines) of Figs. 1 and 2 in the large z region will also be strongly affected and modified by the higher order corrections. For the color-octet ^3P_J processes, on the other hand, their contributions are always smaller than the color-octet $^1S_0$ contributions. And especially, their contributions at large z are similar to the color-singlet contributions, i.e., fall down rapidly with z at the end point region. This property is quite different from their contributions to the unpolarized cross section of J/ψ photoproduction [10,17], which also rise rapidly at large z like the color-octet $^1S_0$ contributions. The p_T^2 distributions of Figs. 1 and 2 are always dominated by the color-octet $^1S_0$ process contributions. And their contributions are larger than the color-singlet contributions by almost an order of magnitude in the whole region of p_T^2, which is similar to their contributions to the unpolarized cross section [10,17]. However, the color-octet ^3P_J contributions to the p_T^2 distributions of the polarized cross sections again have different features compared to their contributions to the unpolarized cross sections [10,17]. Their contributions are much smaller than the color-octet $^1S_0$ contributions in the whole region of p_T^2, and even smaller than the color-singlet contributions at low p_T^2. At very low p_T^2 ($p_T^2 \sim 1 GeV^2$), their contributions to the polarized cross section $\Delta\sigma$ even give a negative

value, which is not plotted in the figures.

In Figs. 3 and 4, we display the asymmetry of Eq. (20) for J/ψ inelastic photoproduction as functions of z and p_T^2. Fig. 3 is for the photon-proton collisions, and Fig. 4 is for the electron-proton collisions. The solid curves are the production asymmetries in the color-singlet model. The other two curves represent the production asymmetries after including the color-octet contributions in two cases of values for the color-octet matrix elements: (I) for the dashed lines, $\langle \mathcal{O}_8^{\psi}(^1S_0)\rangle = 3.0\times 10^{-2} GeV^3$ and $\langle \mathcal{O}_8^{\psi}(^3P_0)\rangle/m_c^2 = 0$; (II) for the dotted lines, $\langle \mathcal{O}_8^{\psi}(^3P_0)\rangle/m_c^2 = 1.0\times 10^{-2} GeV^3$ and $\langle \mathcal{O}_8^{\psi}(^1S_0)\rangle = 0$. The three curves in each diagram have the same behaviors as each other. For the z distributions, the asymmetries for all of the curves rise with z, and then fall down after reaching their maximum values. There is no steep rising as in the polarized and unpolarized cross section distributions when z approaches its end point for all curves. In the whole region of z, the case (I) color-octet predictions are larger than the color-singlet predictions, and the case (II) color-octet predictions on the other hand are similar to the color-singlet predictions in the lower z region and even smaller in the larger z region. For the p_T^2 distributions, the asymmetries for the three curves all rise with p_T^2. The case (I) predictions are similar to the color-singlet predictions. However, the case (II) predictions are smaller than the color-singlet predictions by almost a factor of two. Especially, in the low p_T^2 ($p_T^2 \sim 1 - 2GeV^2$) region, the production asymmetry A for case (II) is very small comparable with zero.

Concluding the results displayed in the above four figures (Figs. 1-4), we can see that the difference between the color-singlet and color-octet predictions on the distributions behaviors and the absolute sizes of the polarized cross sections $\Delta\sigma$ and the production asymmetries A may provide some information on J/ψ production mechanism. That is to say, the inelastic J/ψ photoproduction in polarized collisions will give another independent test for the color-octet mechanism. In particular, as shown in the above analysis, the different features of the contributions from the two different color-octet processes may provide further important informations on the mechanism for the inelastic photoproduction of J/ψ.

Comparing the results of Figs. 3 and 4, we can see that the production asymmetries for the polarized electron-proton collisions are all smaller than those for the polarized photon-proton collisions by about one order of magnitude. This is mostly because the polarized flux factor $\Delta f_{\gamma}^{(e)}$ in Eq. (4) has a minus sign in the coefficient before the logarithmic term (the dominant term) compared with the unpolarized flux factor $f_{\gamma}^{(e)}$ in Eq. (2), which will result in a big difference between them when convoluted with the photoproduction cross section by using Eqs. (6) and (7).

Now, we turn to study the dependence of our results on the different parameterizations for the polarized gluon distributions in the proton. In Fig. 5 and 6, we plot the production asymmetry of J/ψ as functions of z and p_T^2 with different sets of the polarized gluon distribution functions [18–20] (for all these sets, we just use the LO results of them). We have tried all of the polarized gluon distribution parametrizations for every sets mentioned above, but found the different parametrizations for each set give the similar results. However, the difference between different sets are much larger. For representation, we choose the polarized gluon distribution function for each set as follows: the GRVS STD parametrization for the GRVS stes (the solid lines), GS-C for the GS sets (the dashed lines), and DSS1 for the DSS sets (the dotted lines). Fig. 5 are the z distributions and Fig. 6 are the p_T^2 distributions: (a) are for the results only from the color-singlet contribution; (b) are for the results after

including the color-octet contributions, where we choose the color-octet matrix elements of $\langle \mathcal{O}_8^{\psi}(^1S_0)\rangle$ and $\langle \mathcal{O}_8^{\psi}(^3P_0)\rangle$ as

$$\langle \mathcal{O}_8^{\psi}(^1S_0)\rangle = \langle \mathcal{O}_8^{\psi}(^3P_0)\rangle/m_c^2 = 0.008.$$

From these two figures, we can see that the difference of the asymmetry A between the different polarized gluon distribution functions is distinctive both for the color-singlet and color-octet predictions. The GRVS STD set give the production asymmetry much larger than those for the other two sets, and the GS-C set and the DDS1 set give similar results for the production asymmetry.

IV. CONCLUSIONS

We have calculated in this paper the inelastic J/ψ production in polarized photon-hadron collisions. We have evaluated the polarized production rate and the production asymmetry at polarized electron-proton colliders relevant to the HERA energy range. We performed our results both for the color-singlet model predictions and the predictions after including the color-octet contributions. We found that the inelastic J/ψ photoproduction in polarized collisions may give another independent test for the color-octet mechanism. Especially, the different features of the contributions from the two different color-octet processes may provide further important informations on the mechanism for the inelastic photoproduction of J/ψ. And most important, we found that the discrepancy on the production asymmetry A between the various sets of the polarized gluon distribution function is distinctive. So, the process studied in this paper may be a candidate process for the measurement of the polarized gluon distribution function in the proton at future polarized HERA collider.

ACKNOWLEDGMENTS

This work was supported in part by the National Natural Science Foundation of China, the State Education Commission of China, and the State Commission of Science and Technology of China.

After the calculation of this paper was finished we found a paper [25], in which a similar process has been considered, but their result is just for polarized J/ψ production at low energies.

REFERENCES

[1] EMC, J. Ashman, et al, Nucl. Phys. **B328**, 1 (1989).

[2] see for exmple, Proceedings of Workshop on Polarized Protons at HERA, DESY-Proceedings-1998-01, Ed. A. De Roeck and T. Gehrmann; Proceedings of the Workshop on Polarized Protons at High Energies – Accelerator Challenges and Physics Opportunities, May 17, 1999, DESY, Hamburg.

[3] M.B. Einhorn and S.D. Ellis, Phys. Rev. **D12**, 2007 (1975); S.D. Ellis et al., Phys. Rev. Lett. **36**; 1263 (1976);C.-H. Chang, Nucl. Phys. **B172**, 425 (1980); E.L. Berger, D. Jones, Phys. Rev. **D23**, 1521 (1981); R. Baier, R. Rückl, Nucl. Phys. **B201**, 1 (1982);

[4] CDF collaboration, F. Abe *et al.*, Phys. Rev. Lett. **69**, 3704 (1992); Phys. Rev. Lett. **71**, 2537 (1993); Phys. Rev. Lett. **79**, 572 (1997); Phys. Rev. Lett. **79**, 578 (1997)

[5] G.T. Bodwin, L. Braaten, and G. P. Lepage, Phys. Rev. D51 1125 (1995).

[6] E. Braaten and S. Fleming, Phys. Rev. Lett. **74**, 3327 (1995); M. Cacciari, M. Greco, M.L. Mangano and A. Petrelli, Phys. Lett. **B356** 553 (1995).

[7] P. Cho and K. Leibovich, Phys. Rev. D**53**, 150 (1996); *ibid*, D**53**, 6203 (1996).

[8] H1 Collab., S. Aid *et al*, Nucl. Phys. **B472**, 3 (1996).

[9] ZEUS Collab., M. Derrick *et al*, DESY-97-147.

[10] M. Cacciari and M. Krämer, Phys. Rev. Lett. **76**, 4128 (1996); P. Ko, J. Lee and H.S. Song, Phys. Rev. **D54**, 4312 (1996); J. Amundson, S. Fleming and I. Maksymyk, Phys. Rev. **D56**, 5844 (1997).

[11] M.Krämer, Nucl. Phys. **B459**, 3 (1996).

[12] B. Cano-Coloma and M.A. Sanchis-Lozano, Nucl. Phys. **B508**, 753 (1997); B.A. Kniehl and G. Kramer, Eur. Phys. J. **C6**, 493 (1999).

[13] K. Sridhar, A.D. Martin and S.J. Stirling, hep-ph/9806253.

[14] C.F. Weizsäcker, Z. Phys. **88**, 612 (1934); E.J. Williams, Phys. Rev. **45**, 729, (1934).

[15] S. Frixione, M.L. Mangano, P. Nason and G. Ridolfi, Phys. Lett. **B319**, 339 (1993).

[16] D. de Florian and S. Fixione, hep-ph/9904320.

[17] M. Beneke, M. Krämer and M. Vänttinen, Phys. Rev. **D57**, 4258 (1998).

[18] M. Glück, E. Reya, M. Stratmann and W. Vogelsang, Phys. Rev. **D53**, 4775 (1996).

[19] T. Gehrmann and W. Stirling, Phys. Rev. **D53**, 6100 (1996).

[20] D. de Florian, O.A. Sampayo and R. Sassot, Phys. Rev. **D57**, 5803 (1998).

[21] J.Ph. Guillet, Z. Phys. **C39**, 75 (1988).

[22] P.De Causmaecker, R.Gastmans, W.Troost, T.T.Wu, Phys. Lett. **B105**, 215 (1981), Nucl. Phys. **B206**, 53 (1982); R.Gastmans, W.Troost, T.T.Wu, Nucl. Phys. **B291**, 731 (1987).

[23] M. Glück, E. Reya and A. Vogt, Z. Phys. **C67**, 433 (1995).

[24] M. Beneke and M. Krämer, Phys. Rev.**D 55**, 5269 (1997).

[25] G. Japaridze, W.-D. Nowak and A. Tkabladze, hep-ph/9908336.

APPENDIX:

In this appendix, we list the polarized and unpolarized cross sections for the different partonic processes of Eq. (11)-(14). For convenience, we define two variables, $P = \hat{s}\hat{t}+\hat{t}\hat{u}+\hat{s}\hat{u}$ and $Q = (\hat{s}+\hat{t})(\hat{s}+\hat{u})(\hat{t}+\hat{u})$.
$\gamma + g \to c\bar{c}(^3S_1, \underline{1}) + g$: the unpolarized cross section,

$$\frac{d\sigma}{dt} = \frac{2M(4\pi)^3\alpha\alpha_s^2 e_c^2}{27\pi\hat{s}^2}\frac{P^2 - M^2\hat{s}\hat{t}\hat{u}}{Q^2}\langle\mathcal{O}_1^\psi(^3S_1)\rangle, \tag{A1}$$

the polarized cross section,

$$\frac{d\Delta\sigma}{dt} = \frac{2M(4\pi)^3\alpha\alpha_s^2 e_c^2\hat{t}\hat{u}}{27\pi\hat{s}^2}\frac{\hat{s}^2 - P}{Q^2}\langle\mathcal{O}_1^\psi(^3S_1)\rangle \tag{A2}$$

$\gamma + g \to c\bar{c}(^3S_1, \underline{8}) + g$: the unpolarized and polarized cross sections are relevant to those for the process $\gamma + g \to c\bar{c}(^3S_1, \underline{1}) + g$ multiplied by the factor

$$\frac{15}{8}\frac{\langle\mathcal{O}_8^\psi(^3S_1)\rangle}{\langle\mathcal{O}_1^\psi(^3S_1)\rangle} \tag{A3}$$

$\gamma + g \to c\bar{c}(^1S_0, \underline{8}) + g$:

$$\frac{d\sigma}{dt} = \frac{3(4\pi)^3\alpha\alpha_s^2 e_c^2\hat{s}\hat{u}}{16\pi\hat{s}^2}\frac{M^8 + \hat{s}^4 + \hat{t}^4 + \hat{u}^4}{M\hat{t}Q^2}\langle\mathcal{O}_8^\psi(^1S_0)\rangle, \tag{A4}$$

$$\frac{d\Delta\sigma}{dt} = \frac{3(4\pi)^3\alpha\alpha_s^2 e_c^2\hat{s}\hat{u}}{16\pi\hat{s}^2}\frac{M^8 + \hat{s}^4 - \hat{t}^4 - \hat{u}^4}{M\hat{t}Q^2}\langle\mathcal{O}_8^\psi(^1S_0)\rangle. \tag{A5}$$

$\gamma + g \to c\bar{c}(^3P_0, \underline{8}) + g$:

$$\begin{aligned}\frac{d\sigma}{dt} = {} & \frac{(4\pi)^3\alpha\alpha_s^2 e_c^2}{4\pi\hat{s}^2Q^2}\langle\mathcal{O}_8^\psi(^3P_0)\rangle[\frac{9M^5\hat{s}\hat{u}}{t} + \frac{\hat{s}\hat{u}\hat{t}^3(2M^4 + 3\hat{t}M^2 + \hat{s}\hat{u})^2}{M^3(\hat{t}+\hat{s})^2(\hat{t}+\hat{u})^2} \\ & + \frac{\hat{s}^3\hat{u}(3\hat{s}^2M^2 - \hat{t}\hat{u}(2M^2 - \hat{s}))^2}{M^3\hat{t}(\hat{t}+\hat{s})^2(\hat{s}+\hat{u})^2} + \frac{\hat{u}^3\hat{s}(\hat{s}\hat{t}(2M^2 - \hat{u}) - 3\hat{u}^2M^2)^2}{M^3\hat{t}(\hat{t}+\hat{s})^2(\hat{s}+\hat{u})^2}],\end{aligned} \tag{A6}$$

$$\begin{aligned}\frac{d\Delta\sigma}{dt} = {} & \frac{(4\pi)^3\alpha\alpha_s^2 e_c^2}{4\pi\hat{s}^2Q^2}\langle\mathcal{O}_8^\psi(^3P_0)\rangle[\frac{9M^5\hat{s}\hat{u}}{t} - \frac{\hat{s}\hat{u}\hat{t}^3(2M^4 + 3\hat{t}M^2 + \hat{s}\hat{u})^2}{M^3(\hat{t}+\hat{s})^2(\hat{t}+\hat{u})^2} \\ & + \frac{\hat{s}^3\hat{u}(3\hat{s}^2M^2 - \hat{t}\hat{u}(2M^2 - \hat{s}))^2}{M^3\hat{t}(\hat{t}+\hat{s})^2(\hat{s}+\hat{u})^2} - \frac{\hat{u}^3\hat{s}(3\hat{u}^2M^2 - \hat{s}\hat{t}(2M^2 - \hat{u}))^2}{M^3\hat{t}(\hat{t}+\hat{s})^2(\hat{s}+\hat{u})^2}].\end{aligned} \tag{A7}$$

$\gamma + g \to c\bar{c}(^3P_1, \underline{8}) + g$:

$$\begin{aligned}\frac{d\sigma}{dt} = {} & \frac{(4\pi)^3\alpha\alpha_s^2 e_c^2\langle\mathcal{O}_8^\psi(^3P_1)\rangle}{2\pi\hat{s}^2Q^4M^3}[\hat{s}^7(\hat{t}^4 + 2\hat{t}^3\hat{u} + 4\hat{t}^2\hat{u}^2 + 2\hat{t}\hat{u}^3 + \hat{u}^4) + \hat{s}^6(\hat{t}+\hat{u})^2 \\ & (3\hat{t}^3 + 7\hat{t}^2\hat{u} + 7\hat{t}\hat{u}^2 - \hat{u}^3) + \hat{s}^5(3\hat{t}^6 + 22\hat{t}^5\hat{u} + 60\hat{t}^4\hat{u}^2 + 76\hat{t}^3\hat{u}^3 + 36\hat{t}^2\hat{u}^4 \\ & + 4\hat{t}\hat{u}^5 - \hat{u}^6) + \hat{s}^4(\hat{t}+\hat{u})(\hat{t}^6 + 12\hat{t}^5\hat{u} + 46\hat{t}^4\hat{u}^2 + 72\hat{t}^3\hat{u}^3 + 32\hat{t}^2\hat{u}^4 + 4\hat{t}\hat{u}^5\end{aligned}$$

$$
\begin{aligned}
&+\hat{u}^6) + 2\hat{s}^3\hat{t}\hat{u}(\hat{t}^6 + 10\hat{t}^5\hat{u} + 38\hat{t}^4\hat{u}^2 + 59\hat{t}^3\hat{u}^3 + 38\hat{t}^2\hat{u}^4 + 10\hat{t}\hat{u}^5 + \hat{u}^6) \\
&+2\hat{s}^2\hat{t}^2\hat{u}^2(\hat{t} + \hat{u})(\hat{t}^4 + 9\hat{t}^3\hat{u} + 20\hat{t}^2\hat{u}^2 + 10\hat{t}\hat{u}^3 + 2\hat{u}^4) + \hat{s}\hat{t}^3\hat{u}^3(\hat{t} + \hat{u})^2 \\
&(2\hat{t}^2 + 9\hat{t}\hat{u} + 2\hat{u}^2) + \hat{t}^4\hat{u}^4(\hat{t} + \hat{u})^3] \qquad \text{(A8)}
\end{aligned}
$$

$$
\begin{aligned}
\frac{d\Delta\sigma}{dt} = &\frac{(4\pi)^3\alpha\alpha_s^2 e_c^2\hat{t}\hat{u}\langle\mathcal{O}_8^{\psi}(^3P_1)\rangle}{2\pi\hat{s}^2Q^3(\hat{t} + \hat{u})M^3}[2\hat{s}^5(\hat{t}^2 + \hat{t}\hat{u} + \hat{u}^2) + 2\hat{s}^4\hat{t}(\hat{t} + \hat{u})(2\hat{t} + 3\hat{u}) \\
&+\hat{s}^3\hat{t}(2\hat{t}^3 + 5\hat{t}^2\hat{u} + 2\hat{t}\hat{u}^2 + \hat{u}^3) - 2\hat{s}^2\hat{u}(\hat{t} + \hat{u})(2\hat{t}^3 + 8\hat{t}^2\hat{u} + 3\hat{t}\hat{u}^2 + \hat{u}^3) \\
&-\hat{s}\hat{t}\hat{u}(\hat{t} + \hat{u})^2(\hat{t}^2 + 7\hat{t}\hat{u} + \hat{u}^2) - \hat{t}^2\hat{u}^2(\hat{t} + \hat{u})^3] \qquad \text{(A9)}
\end{aligned}
$$

$\gamma + g \to c\bar{c}(^3P_2, \underline{8}) + g$:

$$
\begin{aligned}
\frac{d\sigma}{dt} = &\frac{(4\pi)^3\alpha\alpha_s^2 e_c^2\langle\mathcal{O}_8^{\psi}(^3P_2)\rangle}{10\pi\hat{s}^2Q^4M^3\hat{t}}[12s^9u(t + u)^2 + 12s^8u(t + u)(5t^2 + 7tu + 4u^2) + s^7(3t^5 \\
&+142t^4u + 384t^3u^2 + 454t^2u^3 + 303tu^4 + 96u^5) + s^6(t + u)(9t^5 + 202t^4u \\
&+438t^3u^2 + 442t^2u^3 + 309tu^4 + 120u^5) + s^5(9t^7 + 198t^6u + 736t^5u^2 + 1200t^4u^3 \\
&+1184t^3u^4 + 860t^2u^5 + 429tu^6 + 96u^7) + s^4(t + u)(3t^7 + 100t^6u + 450t^5u^2 \\
&+720t^4u^3 + 688t^3u^4 + 496t^2u^5 + 255tu^6 + 48u^7) + 2s^3u(11t^8 + 114t^7u + 362t^6u^2 \\
&+585t^5u^3 + 600t^4u^4 + 440t^3u^5 + 227t^2u^6 + 66tu^7 + 6u^8) + 2s^2tu^2(t + u)^2(19t^5 \\
&+76t^4u + 104t^3u^2 + 84t^2u^3 + 48tu^4 + 12u^5) + st^2u^3(t + u)^2(22t^4 + 59t^3u \\
&+58t^2u^2 + 36tu^3 + 12u^4) + 3(t + u)^3t^5u^4], \qquad \text{(A10)}
\end{aligned}
$$

$$
\begin{aligned}
\frac{d\Delta\sigma}{dt} = &\frac{(4\pi)^3\alpha\alpha_s^2 e_c^2\hat{u}\langle\mathcal{O}_8^{\psi}(^3P_2)\rangle}{10\pi\hat{s}^2Q^3M^3\hat{t}(\hat{t} + \hat{u})}[12s^7(t + u)^2 + 12s^6(t + u)(4t^2 + 5tu + 3u^2) + 2s^5(41t^4 \\
&+99t^3u + 107t^2u^2 + 78tu^3 + 30u^4) + 6s^4(t + u)(12t^4 + 21t^3u + 24t^2u^2 + 20tu^3 \\
&+10u^4) + s^3(30t^6 + 117t^5u + 226t^4u^2 + 285t^3u^3 + 228t^2u^4 + 108tu^5 + 24u^6) \\
&+2s^2t(t + u)^2(2t^4 + 16t^3u + 20t^2u^2 + 13tu^3 + 6u^4) + st^2u(t + u)^2(7t^3 + 5t^2u \\
&-17tu^2 - 12u^3) + 3t^4u^2(t + u)^3]. \qquad \text{(A11)}
\end{aligned}
$$

In practice, the three $^3P_J^{(8)}$ ($J = 0,\ 1,\ 2$) subprocesses contributions to J/ψ production are always added together, by using the relation of their color-octet matrix elements due to the heavy quark spin symmetry Eq. (25). For convenience, we also give here the total sum of the cross sections for the three $^3P_J^{(8)}$ processes, which is more simpler than the above expressions.

The sum of the three $^3P_J^{(8)}$ subprocesses,

$$
\begin{aligned}
\frac{d\sigma(^3P_J^{(8)})}{dt} = &\frac{3(4\pi)^3\alpha\alpha_s^2 e_c^2\langle\mathcal{O}_8^{\psi}(^3P_2)\rangle}{2\pi\hat{s}^2Q^3M^3\hat{t}}[7\hat{s}^7\hat{u}(\hat{t} + \hat{u}) + \hat{s}^6\hat{u}(25\hat{t}^2 + 38\hat{t}\hat{u} + 21\hat{u}^2) \\
&+\hat{s}^5(\hat{t} + \hat{u})(2\hat{t}^3 + 45\hat{t}^2\hat{u} + 43\hat{t}\hat{u}^2 + 35\hat{u}^3) + \hat{s}^4(4\hat{t}^5 + 63\hat{t}^4\hat{u} + 132\hat{t}^3\hat{u}^2 \\
&+156\hat{t}^2\hat{u}^3 + 98\hat{t}\hat{u}^4 + 35\hat{u}^5) + \hat{s}^3(\hat{t} + \hat{u})(2\hat{t}^5 + 45\hat{t}^4\hat{u} + 91\hat{t}^3\hat{u}^2 + 99\hat{t}^2\hat{u}^3 \\
&+57\hat{t}\hat{u}^4 + 21\hat{u}^5) + \hat{s}^2\hat{u}(13\hat{t}^6 + 70\hat{t}^5\hat{u} + 136\hat{t}^4\hat{u}^2 + 132\hat{t}^3\hat{u}^3 + 88\hat{t}^2\hat{u}^4 \\
&+38\hat{t}\hat{u}^5 + 7\hat{u}^6) + \hat{s}\hat{t}\hat{u}^2(\hat{t} + \hat{u})(13\hat{t}^4 + 34\hat{t}^3\hat{u} + 29\hat{t}^2\hat{u}^2 + 18\hat{t}\hat{u}^3 + 7\hat{u}^4) \\
&+2\hat{t}^4\hat{u}^3(\hat{t} + \hat{u})^2], \qquad \text{(A12)}
\end{aligned}
$$

$$\frac{d\Delta\sigma(^3P_J^{(8)})}{dt} = \frac{-3(4\pi)^3\alpha\alpha_s^2 e_c^2\hat{u}\langle\mathcal{O}_8^{\psi}(^3P_2)\rangle}{2\pi\hat{s}^2Q^3M^3\hat{t}}[\hat{s}^7(\hat{t}+\hat{u})+\hat{s}^6(7\hat{t}^2+2\hat{t}\hat{u}+3\hat{u}^2)+\hat{s}^5(\hat{t}+\hat{u})$$
$$(11\hat{t}^2-17\hat{t}\hat{u}+5\hat{u}^2)+\hat{s}^4(9\hat{t}^4-28\hat{t}^3\hat{u}-48\hat{t}^2\hat{u}^2-26\hat{t}\hat{u}^3+5\hat{u}^4)$$
$$+\hat{s}^3(\hat{t}+\hat{u})(8\hat{t}^4-19\hat{t}^3\hat{u}-37\hat{t}^2\hat{u}^2-23\hat{t}\hat{u}^3+2\hat{u}^4)+\hat{s}^2\hat{t}(2\hat{t}+\hat{u})$$
$$(2\hat{t}^4+7\hat{t}^3\hat{u}-2\hat{t}^2\hat{u}^2-19\hat{t}\hat{u}^3-8\hat{u}^4)+\hat{s}\hat{t}^2\hat{u}(\hat{t}+\hat{u})(6\hat{t}^3+6\hat{t}^2\hat{u}$$
$$-13\hat{t}\hat{u}^2-10\hat{u}^3)+2\hat{t}^4\hat{u}^2(\hat{t}+\hat{u})^2]. \qquad \text{(A13)}$$

Figure Captions

FIG. 1. The polarized cross section distribution as a function of (a) z and (b) p_T^2 in polarized photon-proton collisions at the energy range of $W_{\gamma p} = 100GeV$.
FIG. 2. The polarized cross section distribution as a function of (a) z and (b) p_T^2 in polarized electron-proton collisions at the energy range relevant to HERA, $\sqrt{s} = 300GeV$, where we use the Weizsäcker-Williams approximation to evaluate the production rate for electron-proton collisions.
FIG. 3. The production asymmetry distributions for Fig. 1.
FIG. 4. The production asymmetry distributions for Fig. 2.
FIG. 5. The z distributions of the production asymmetry A for the inelastic J/ψ photoproduction in polarized electron-proton collisions for different sets of polarized gluon distribution in the proton. (a) are the results for the color-singlet predictions, and (b) are the results after including the color-octet contributions.
FIG. 6. The same as Fig. 5, but for the p_T^2 distributions.

γp collisions, E_{cm}=100GeV, GRVS STD

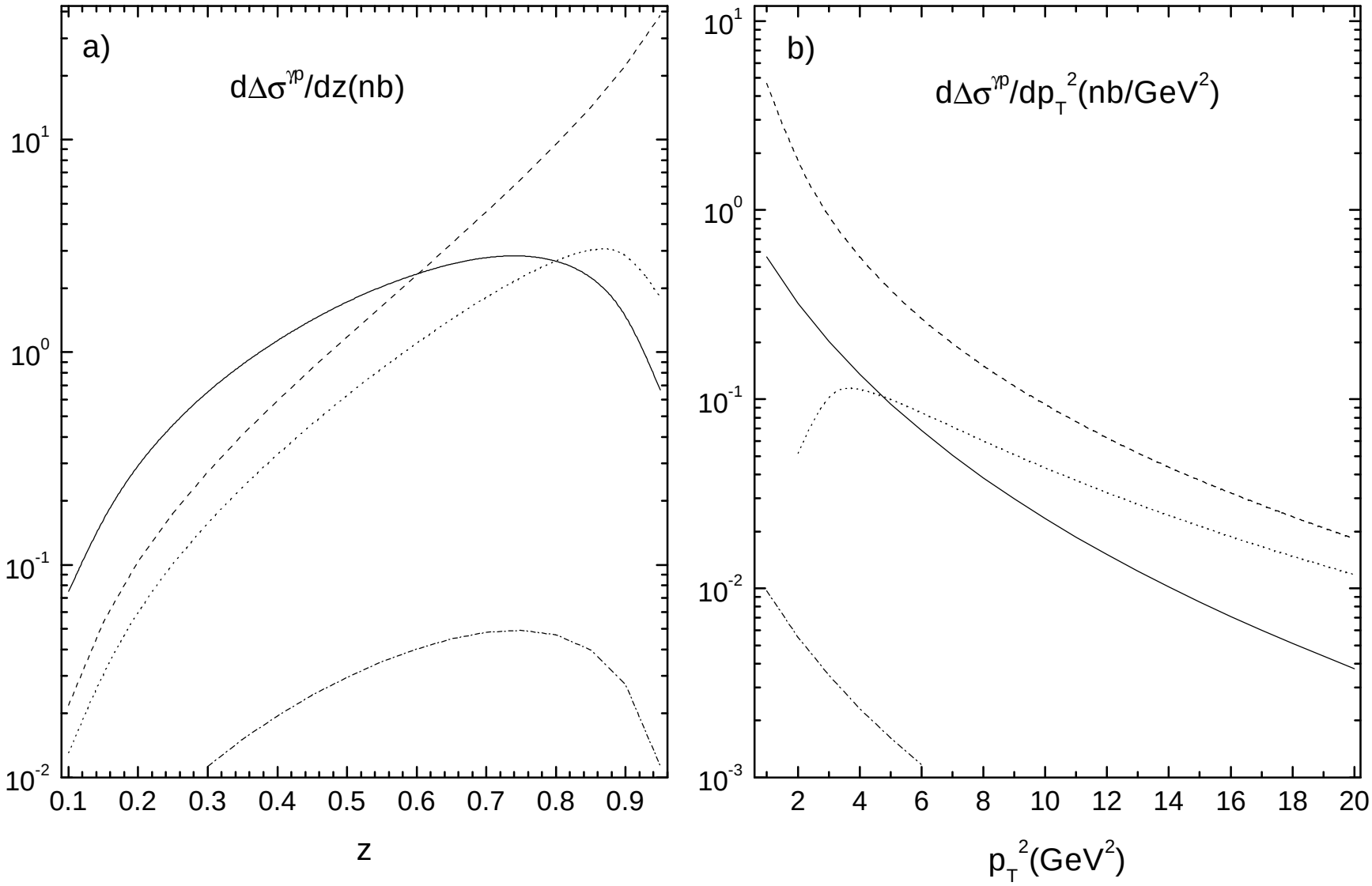

Fig.1

ep collisions, E_{cm}=300GeV, GRVS STD

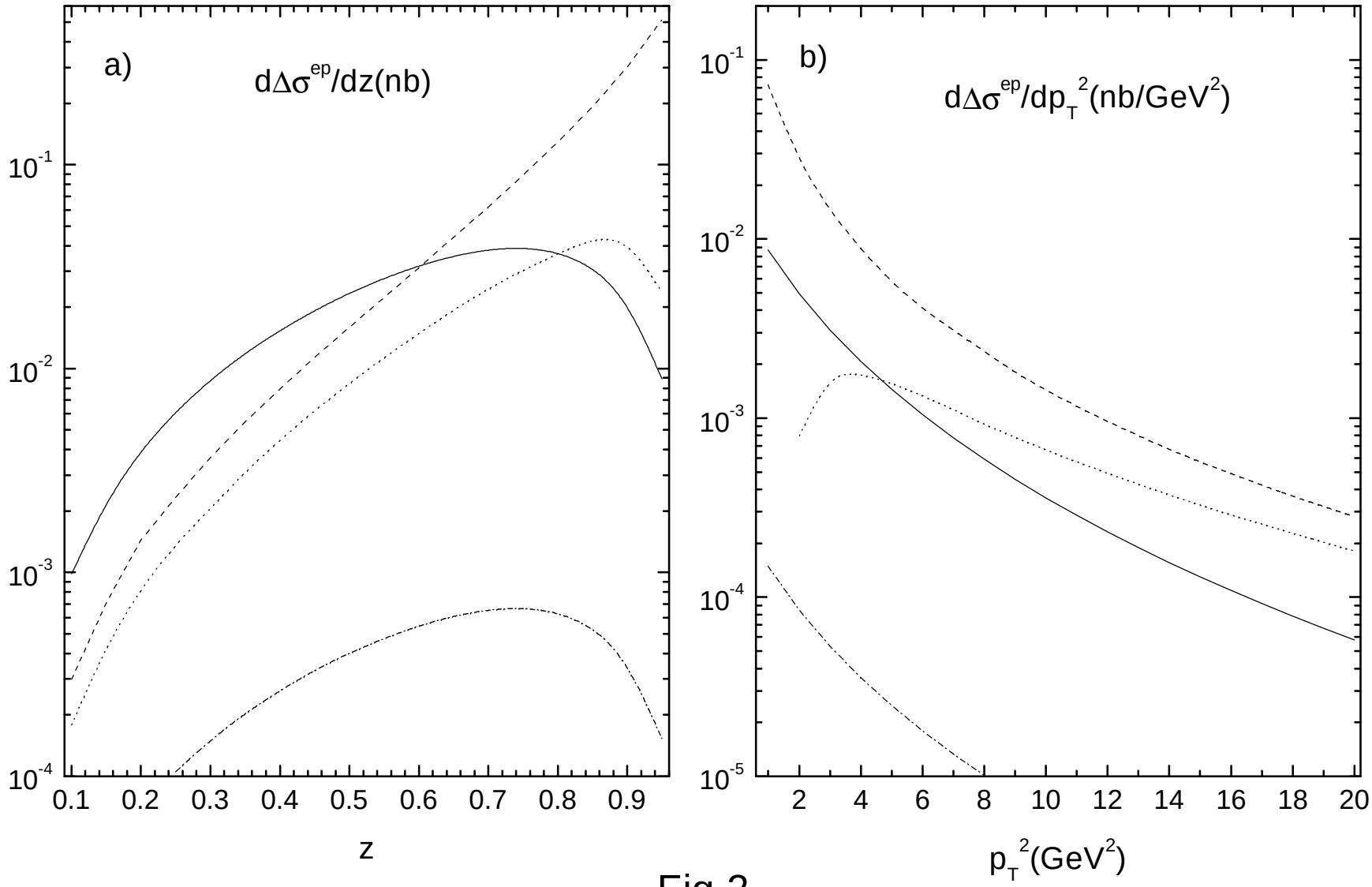

Fig.2

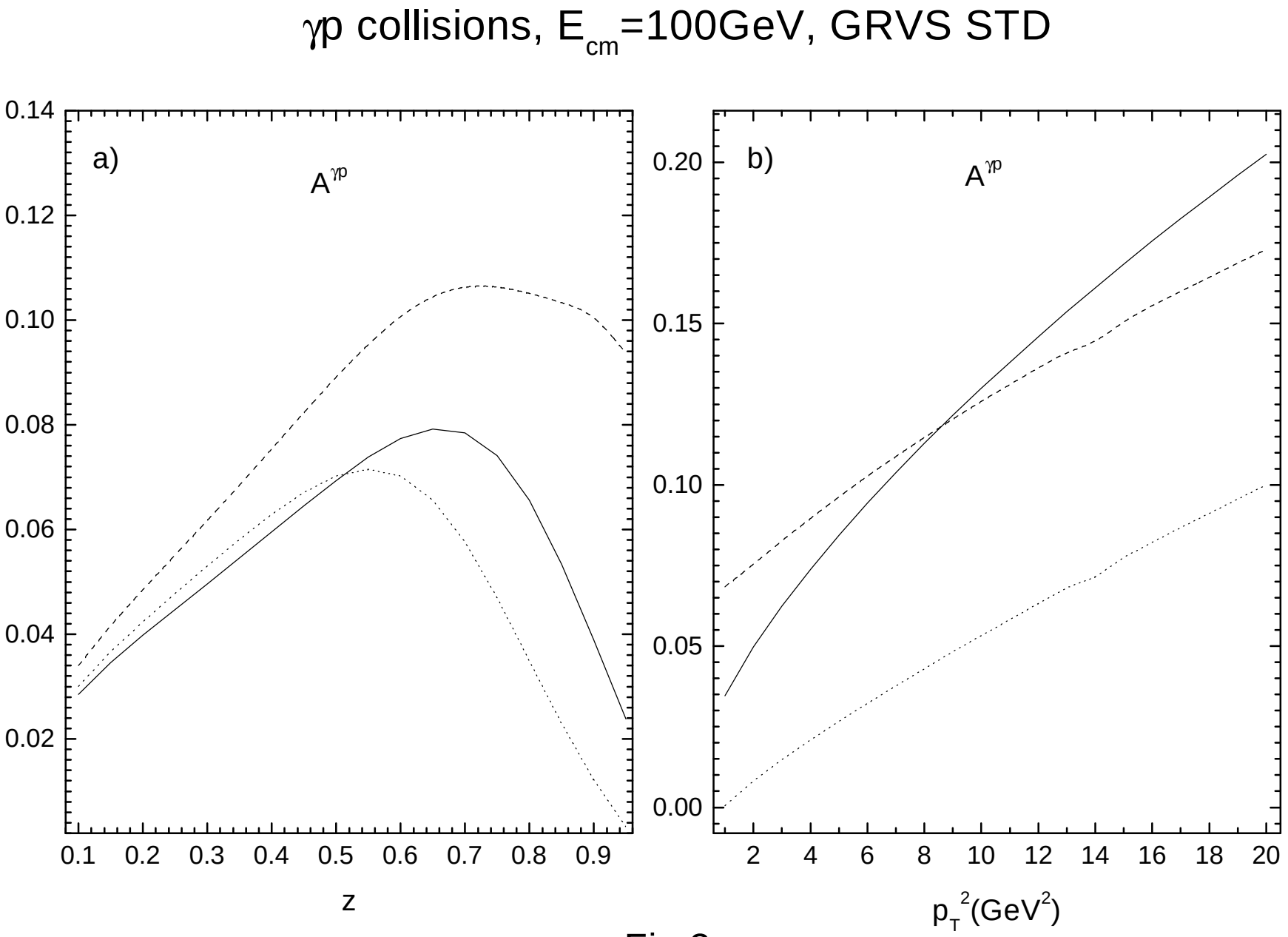
γp collisions, E_cm=100GeV, GRVS STD
a)
A^γp
0.14
0.12
0.10
0.08
0.06
0.04
0.02
0.1
0.2
0.3
0.4
0.5
0.6
0.7
0.8
0.9
z
b)
A^γp
0.20
0.15
0.10
0.05
0.00
2
4
6
8
10
12
14
16
18
20
p_T^2(GeV^2)

Fig.3

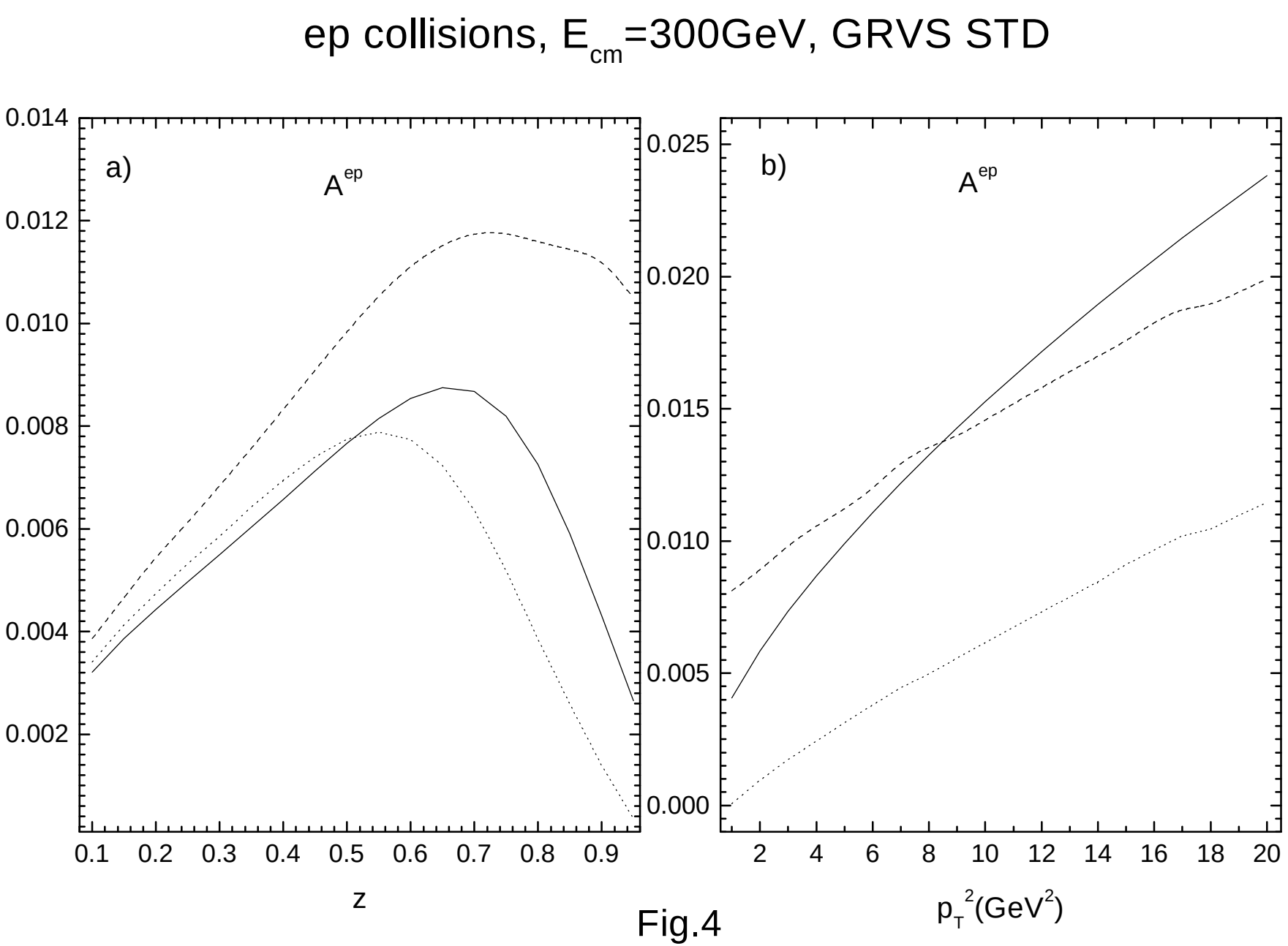
ep collisions, E_cm=300GeV, GRVS STD
a)
A^ep
0.014
0.012
0.010
0.008
0.006
0.004
0.002
0.1
0.2
0.3
0.4
0.5
0.6
0.7
0.8
0.9
z
b)
A^ep
0.025
0.020
0.015
0.010
0.005
0.000
2
4
6
8
10
12
14
16
18
20
p_T^2(GeV^2)

Fig.4

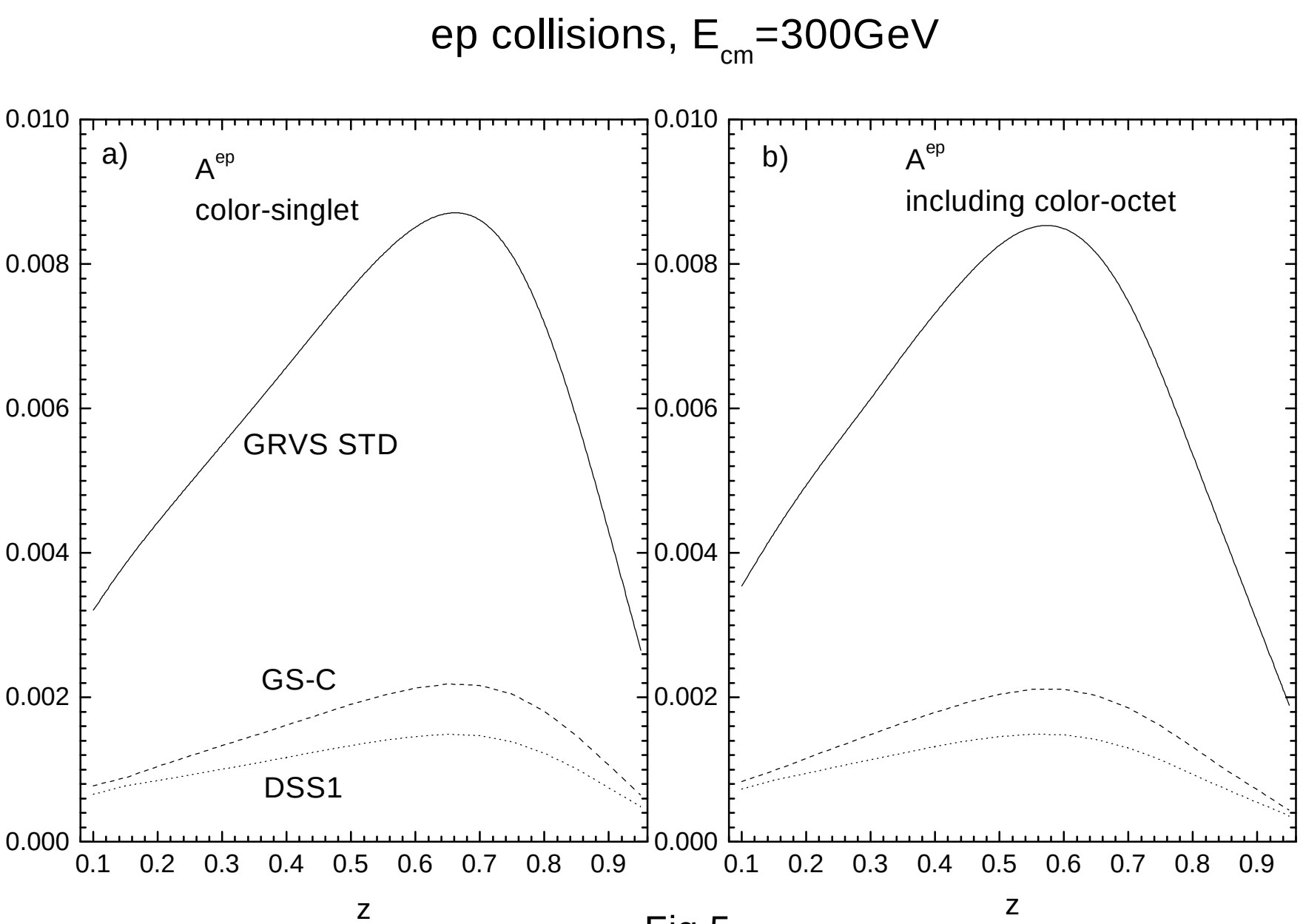
ep collisions, E_cm=300GeV
a)
A^ep
color-singlet
GRVS STD
GS-C
DSS1
b)
A^ep
including color-octet
0.010
0.008
0.006
0.004
0.002
0.000
0.1
0.2
0.3
0.4
0.5
0.6
0.7
0.8
0.9
z

Fig.5

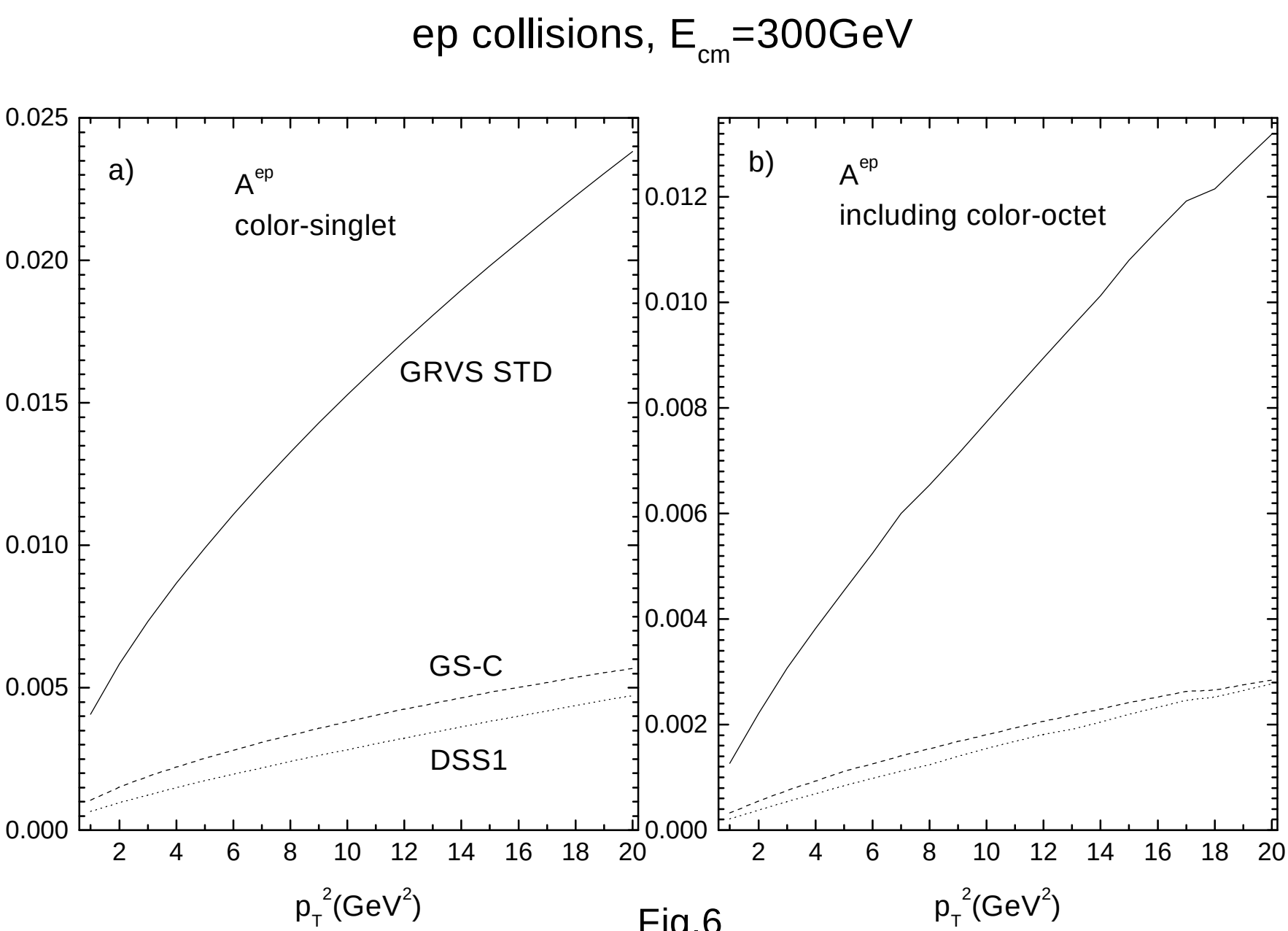
ep collisions, E_cm=300GeV
a)
A^ep
color-singlet
GRVS STD
GS-C
DSS1
b)
A^ep
including color-octet
p_T^2(GeV^2)
p_T^2(GeV^2)

Fig.6